Materials Science and Engineering A366 (2004) 229–238

www.elsevier.com/locate/msea

X-ray diffraction line profile analysis of iron ball milled powders

S. Vives [a,*], E. Gaffet [b], C. Meunier [a]

[a] CREST, UMR-6000 CNRS, UFC-UTBM, Pôle Universitaire, 4 Place Tharradin, BP 71427, 25211 Montbéliard Cedex, France
[b] UPR-806 CNRS, Groupe "Nanomatériaux: Elaboration et Transitions de Phases Hors Equilibre" UTBM, Site de Sévenans, 90010 Belfort Cedex, France

Received 19 July 2002; received in revised form 3 July 2003

Abstract

The size of coherently diffracting domains and the lattice strain of iron ball milled powders have been determined according to various models. The Williamson–Hall plot, the Voigt model and the Warren–Averbach model have been employed. The analytical expressions of the size and strain Fourier coefficients have been extracted from the integral breadth using the so-called "double Voigt" method. The shock power generated in the planetary ball milling equipment employed has been calculated for each synthesis condition and used to plot the size and the strain. The nature (screw or edge) and the density of the dislocations have been determined for each powder under investigation.

Keywords: X-ray line profile analysis; Ball milling; Iron

1. Introduction

Nanocrystalline materials obtained by high-energy ball milling are of great interest since it is known that those materials may exhibit different physico-chemical properties than the coarse grain similar materials. Various equipments are available to perform ball milling experiments such as attritor, shake miller and planetary ball miller. This last device is now largely employed to obtained nanocrystalline powders. In order to correlate the microstructure of such powders with their properties it is necessary to use methods allowing meaningful results about size and strain.

X-rays diffraction line profile analysis (LPA) is an adapted tool to characterize the behavior of a metallic powder under various high-energy ball milling conditions. In almost all the works related to ball milling process, authors give results about the size–strain analysis and they often correlated those results with physical properties (mechanical or magnetic) of the resulting materials. Among all the methods existing to extract the size of the coherent diffracting domains from diffraction peak the Scherrer relation [1] is still the most employed nowadays [2–7]. Scherrer gave a definition of the "apparent" domain size that is a volume-weighted quantity:

$$t = \frac{K\lambda}{\mathrm{FWHM}}\cos\theta \tag{1}$$

where K is a constant close to unity, FWHM corresponds to the full width at half maximum of the peak and θ the Bragg angle of the $[h\,k\,l]$ reflection.

Later Wilson [8] defined an "integral breadth apparent size" that is also a volume-weighted quantity:

$$\langle D\rangle_v = \frac{K\lambda}{\beta}\cos\theta \tag{2}$$

where the integral breadth $\beta = A/I_0$, A being the peak area and I_0 the height of the observed line profile. In these two relations the peak broadening is attributed to the effect of the diffracting coherent domain size.

If the broadening is now due to the sole strain effect, the relations defined by Stokes and Wilson [9] can be applied:

$$\eta = \beta\cot\theta \tag{3}$$

$$e = \frac{\eta}{4} = \frac{\beta}{4}\tan\theta \tag{4}$$

where η is the "apparent" strain and e the maximum strain.

In almost all cases line broadening occurs due to simultaneously size and lattice distortion effects. One way to separate these two effects has been developed by Williamson and Hall [10] and is now known as the Williamson–Hall plot.

* Corresponding author. Tel.: +33-381-994-668; fax: +33-381-994-673.
E-mail address: serge.vives@pu-pm.univ-fcomte.fr (S. Vives).

0921-5093/$ – see front matter © 2003 Elsevier B.V. All rights reserved.
doi:10.1016/S0921-5093(03)00572-0

They proposed to plot β for all the reflections of the sample, expressed in terms of reciprocal unit ($\beta^* = \beta\cos(\theta)/\lambda$), as a function of d^* ($d^* = 2\sin(\theta)/\lambda$). Using a linear extrapolation to this plot, the intercept gives the particle size ($K/\langle D\rangle_v$) and the slope gives the strain (2η). This method can be used quantitatively only in a first approximation due to the fact that the assumption that broadening functions (size and strain) are Cauchy curves is never confirmed in practice. This method is still largely employed for the ball milled samples [11–16] and program softwares are available to perform Williamson–Hall plot [17,18].

Langford [19] proposed to use the Voigt function to fit the diffraction line profile. The Voigt function is a convolution of a Lorentzian (L) function and a Gaussian (G) function. De Keijser et al. [20], in the case of a single line analysis, assumed that the Lorentz component of the line profile is solely due to the crystallite size and that the Gaussian contribution arises from the strain. Hence the apparent domain size for a $h\,k\,l$ reflection can be deduced using the relation (2) replacing β by β_{L} and the strain is obtained using the relation (4) replacing β by β_{G}, β_{L} and β_{G} being the Lorentzian and Gaussian parts of the integral breadth. β can also be used in the Williamson–Hall plot to reveal any structural imperfections [21].

It is also possible to separate the effects of particle size and microstrain on the line broadening using the Warren–Averbach method [22]. In this method, it is shown that the cosine Fourier coefficients A_L of the profile are the product of the size coefficients A_L^{S} and the distortion coefficients A_L^{D}:

$$A_L = A_L^{\mathrm{S}} A_L^{\mathrm{D}} \tag{5}$$

L is the Fourier length, defined as $L = na_3$, where n is the integer and a_3 the unit of the Fourier length in the direction of the diffraction vector $\boldsymbol{g}$:

$$a_3 = \frac{\lambda}{2(\sin\theta_2 - \sin\theta_1)} \tag{6}$$

where the line profile is measured from θ_1 to θ_2 and λ is the wavelength of the X-rays. Warren has shown that the Fourier coefficients can be written as:

$$\ln A_L(\boldsymbol{g}) \simeq \ln A_L^{\mathrm{S}} - 2\pi^2 L^2 \boldsymbol{g}^2 \langle \varepsilon_{\boldsymbol{g}}^2 \rangle \tag{7}$$

where $\langle \varepsilon_{\boldsymbol{g}}^2 \rangle$ is the mean square strain in the direction of the diffraction vector. For a cubic crystal $1/\boldsymbol{g} = d = a/h_0$ where $h_0 = h^2 + k^2 + l^2$ and the last expression becomes:

$$\ln A_L(h_0) = \ln A_L^{\mathrm{S}} - 2\pi^2 \langle \varepsilon_L^2 \rangle L^2 \frac{h_0^2}{a^2}. \tag{8}$$

If two orders of a reflection are available we can plot $\ln A_L$ against h_0^2, the intercept at $h_0^2 = 0$ will give the size coefficients A_L^{S} and the slope will yield the root mean square strain (RMSS) component $\langle \varepsilon_L^2 \rangle^{1/2}$. Once those coefficients obtained we can plot A_L^{S} against L, Warren and Averbach have demonstrated that the intercept of the initial slope on the L-axis directly gives the average column length $\langle D\rangle_{\mathrm{s}}$, also called the surface averaged (or weighted) crystallite size. The Warren–Averbach method is employed in the field of ball milled materials [23–25] and is sometime compared with the results obtained using the Scherrer relation or the Voigt method [26,27].

In addition to the line broadening due to the particle size and strain, there is a source of broadening due to the equipment itself (slit size, penetration in the sample, imperfect focusing ...). This source of broadening is called "instrumental broadening". A correction for the contribution of the instrumental broadening can be made considering that the experimental profile $h(x)$ is a convolution of the sample profile $f(x)$ and the instrumental contribution $g(x)$.

$$h(x) = f(x) \otimes g(x) \tag{9}$$

Using the properties of Fourier series, Stokes [28] demonstrated that $f(x)$ could be obtained from the Fourier coefficient of $\boldsymbol{g}(x)$ and $h(x)$. The $g(x)$ profile is obtained through the acquisition, in the same conditions as the experimental profile $h(x)$, of a standard sample.

Another way to have information about $f(x)$ is to assume that each function (f, g, h) is a Voigt function. The Voigt function being a convolution of a Lorentzian (L) function and a Gaussian (G) function, from Eq. (9) we obtain [21]:

$$\beta_{f\mathrm{L}} = \beta_{h\mathrm{L}} - \beta_{g\mathrm{L}} \tag{10a}$$

and

$$\beta_{f\mathrm{G}}^2 = \beta_{h\mathrm{G}}^2 - \beta_{g\mathrm{G}}^2 \tag{10b}$$

$\beta_{i\mathrm{G}}$ and $\beta_{i\mathrm{L}}$ being the Gaussian and the Lorentzian components of the integral breadth of the profile $i(x)$.

β_f is then obtained using a calibration graph [19] or by an approximation using the relation [20]:

$$\frac{\beta_{f\mathrm{G}}}{\beta_f} = -\tfrac{1}{2}\pi^{1/2}k + \tfrac{1}{2}(\pi k^2 + 4)^{1/2} - 0.234k\exp(-2.176k) \tag{11}$$

with $k = \beta_{f\mathrm{L}}/\pi^{1/2}\beta_{f\mathrm{G}}$.

Furthermore fitting the diffraction peaks by Voigt functions allows the determination of the Fourrier size and strain coefficient using the so-called "double Voigt" method [29]. The main relations in this method are:

$$\beta_{\mathrm{C}} = \beta_{\mathrm{CS}} + \beta_{\mathrm{CD}}\frac{s^2}{s_0^2} \tag{12a}$$

$$\beta_{\mathrm{G}}^2 = \beta_{\mathrm{GS}}^2 + \beta_{\mathrm{GD}}^2\frac{s^2}{s_0^2} \tag{12b}$$

with $s = 2\sin(\theta)/\lambda = 1/d$ being a variable in reciprocal space.

The unknowns β_{CS}, β_{CD}, β_{GS} and β_{GD} are obtained by plotting both β_{C} and β_{G}^2 as a function of s^2 for multiple orders of a reflection. It then possible to have an analytical

expression of the Fourier size coefficients and of the strain ones:

$$A_L^S = \exp(-2L\beta_{CS} - \pi L^2 \beta_{GS}^2) \quad (13)$$

$$\langle \varepsilon_L^2 \rangle = \frac{1}{s^2}\left(\frac{\beta_{GD}^2}{2\pi} + \frac{\beta_{CD}}{\pi^2}\frac{1}{L}\right). \quad (14)$$

In order to prevent the "hook" effect to appear the following condition must be fulfilled:

$$\beta_{CS} = \left(\frac{\pi}{2}\right)^{12} \beta_{GS}. \quad (15)$$

We have decided in this work to compare the results concerning the size–strain analysis obtained from the four methods (Scherrer relation, Williamson–Hall plot, Voigt method and Warren–Averbach method). The choice of using the Voigt function to fit all the diffraction peaks has also be made knowing that all the parameters necessary to perform the different analysis are easily obtained. We have also compared those results with the data arising from the modified Williamson–Hall plot and the modified Warren–Averbach method. The mechanical parameters of the planetary ball miller have been calculated to discuss the different results.

Finally, due to its high use in powder metallurgy, we have chosen to study the evolution of the size and the microstrain of an iron ball milled powder.

2. Experimental

2.1. Milling conditions

Fe powders are milled in a G5 planetary ball mill, this equipment allows the variation of the disk and the vial rotation speeds independently. The disk and the vial radius are, respectively, 132×10^{-3} and 21×10^{-3} m. The ball radius and the ball mass are, respectively, 7.5×10^{-3} m and 14 g, five balls are used in each run. In order to study the effect of the disk rotation speed, the vial rotation speed is fixed at −400 rpm and the disk rotation speed takes the values 150, 250, 350 rpm, the milling time is then fixed at 24 h.

2.2. X-ray diffraction conditions

Data have been recorded using an X'PERT MPD $\theta/2\theta$ (Philips) diffractometer in a parafocusing configuration with Cu Kα radiation. The primary optic is equipped with Soller slits (0.04 rad); an anti-divergence slit (1°) and the secondary optic is equipped with a receiving slit (0.15°), Soller slits (0.04 rad), a curved Si monochromator and a proportional detector.

The acquisition conditions are listed in Table 1. The Cu Kα2 radiation was analytically suppressed from the profile using the Rachinger method.

Table 1
Conditions for the diffraction acquisitions

h k l	Standard position (°2θ)	Range (°2θ)	Step size (°2θ)	Step time (s)
1 1 0	44.674	43–46.5	0.02	40
2 0 0	65.023	63–67	0.02	40
2 1 1	82.335	80.5–84.5	0.02	40
2 2 0	98.949	97–101	0.02	40
3 1 0	116.39	113.5–120	0.05	40
2 2 2	137.144	134–141	0.05	40

3. Results and discussion

Before performing the profile line analysis, we have first calculated the evolution of the lattice parameter of the Fe powder before and after ball milling. The lattice parameter is determined from the average of the parameter calculated from each diffraction peak. The results are given in Fig. 1, the line represents the value of the Fe lattice parameter ($a = 2.8664$ Å) given in the JCPDS database. We observe the increase of the lattice parameter that could be due to the surface energy of the crystals that reach high values when the size decreases leading to the expansion of the cell.

Whatever the method employed, we have seen that the first step of a line profile analysis is to record reflections from a standard sample. One way to know if a sample will be a correct standard is to plot the full width at half maximum of the reflections of this sample against the peaks positions (°2θ). This curve is called the Instrument Resolution Function (IRF) [21]. In Fig. 2 such functions are shown for three samples, a standard Si powder, a well-annealed Fe powder and the starting Fe powder used in this study. We observe that the Fe starting powder displays a greater broadening than the well-annealed Fe and the standard Si powders implying that in this powder size and strain effects are present and cannot be neglected. Hence we have chosen the well-annealed Fe powder as a standard even if broadening is a little more pronounced than in the Si powder. This choice is motivated by the fact that the standard and the powders under investigation are the same material with peaks positions very close (the same 2θ scan range) and the same X-ray absorption coefficient.

In order to use the Williamson–Hall plot for a rapid comparison of size and strains between the different milling conditions, all the peaks have been fitted by Voigt functions and we used Eqs. (10) and (11) to obtain the integral breadths β_f. An example of such a fit is presented in Fig. 3 The Williamson–Hall plots for the starting Fe powders and the three ball milled powders are given in Fig. 4. As it can be seen the (2 0 0) and (3 1 0) reflections are broader than the others reflections. This could be due, firstly to a slight tetragonal distortion [11,30] and secondly to the difference of the elastic moduli of single crystal Fe existing between the (2 0 0) and (3 1 0) and the others crystallographic directions [12,31]. We have thus decided to exclude the (2 0 0) and (31 0) reflections for the Williamson–Hall plots. The

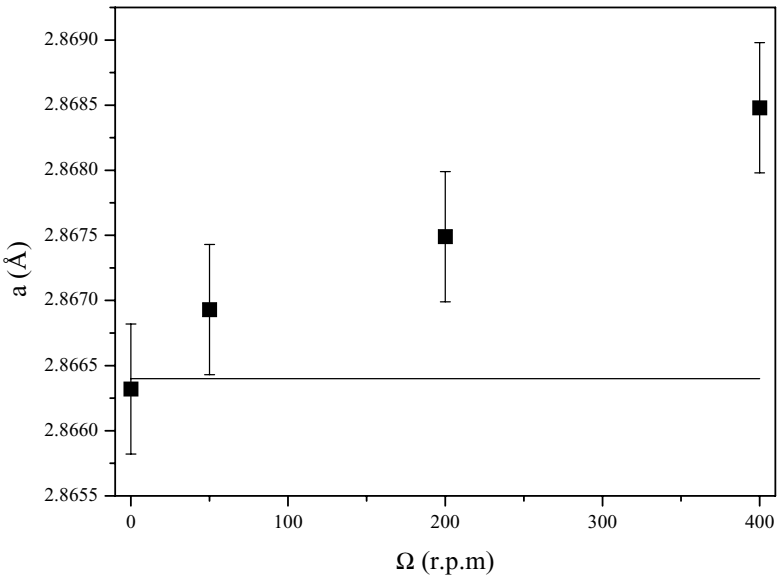

Fig. 1. Evolution of the Fe lattice parameter with the milling conditions.

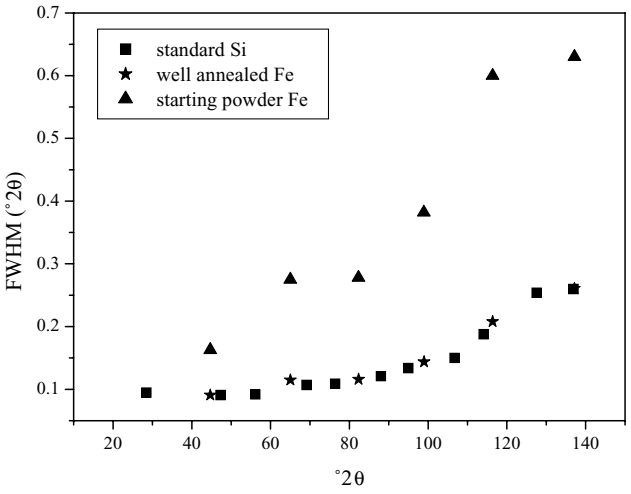

Fig. 2. Intensity Resolution Function (IRF).

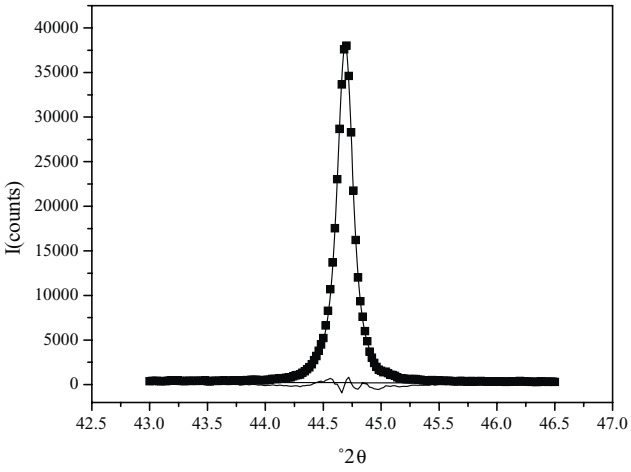

Fig. 3. Fit with a Voigt function of the starting Fe powder: (1 1 0) reflection.

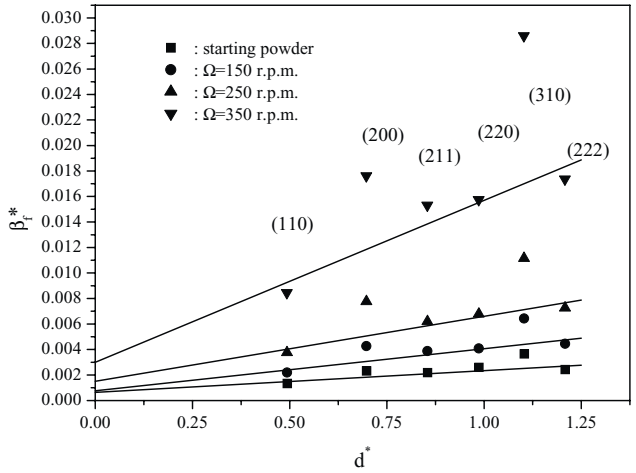

Fig. 4. Williamson–Hall plots ($\omega = -400$ rpm) for the different disk speed conditions.

results of these plots summarized in Table 2 illustrate the influence of the disk speed on the size and the strain of the Fe ball milled powders.

We have then calculated the size and strain Fourier coefficients using the Stoke deconvolution [28] and the Warren–Averbach method (Eqs. (5)–(8)) for the (1 1 0) and (2 2 0) reflections. We have obtained A^S coefficients with

Table 2
Results for the Williamson–Hall plots

Disk speed (Ω) (rpm)	Size ($\langle D \rangle_v$) (Å)	Strain (η)
Starting powder	1393	0.85×10^{-3}
150	1189	1.65×10^{-3}
250	600	2.55×10^{-3}
350	300	6.35×10^{-3}

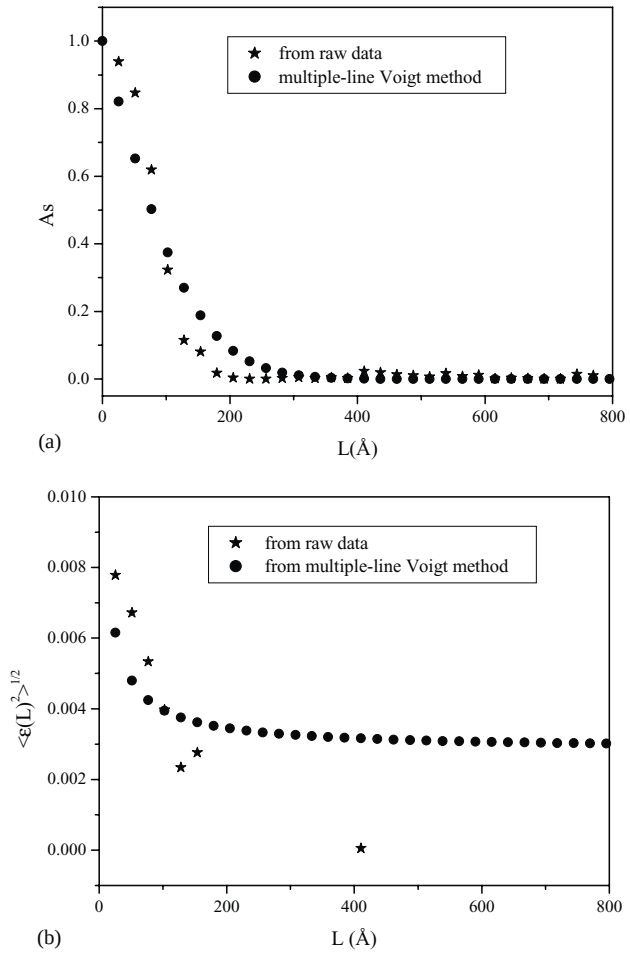

Fig. 5. A^S (a) and strain (b) coefficients obtained from raw data and the multiple-line Voigt method for $\Omega = 350$ rpm.

a strong "hook" effect and RMSS ($\langle\varepsilon_L^2\rangle^{1/2}$) with scattered data as it can be seen in Fig. 5. One way to attain higher quality data is to use the so-called multiple-line Voigt method [29]. Expressions (12), (13) and (14) have been used and results are presented in Fig. 5 for the sample milled at $\Omega = 350$ rpm. No "hook" effect is observed for the A^S coefficients and monotically decreasing curves are obtained. Furthermore it is possible from β_{CS}, β_{CD}, β_{GS}, β_{GD} and from the A_L^S expressions to directly calculate the average surface-weighted domain size $\langle D\rangle_s$ (consistent with the Warren–Averbach formalism), the average volume-weighted domain size $\langle D\rangle_v$ (consistent with the Scherrer equation), and the surface-weighted and volume-weighted column length distribution functions $p_s(L)$ and $p_v(L)$. Expression of $\langle D\rangle_s$, $\langle D\rangle_v$, $p_s(L)$ and $p_v(L)$ can be found in [29]. It is also possible to calculate the maximum strain e (see Eq. (4)) that will be a function of β_D. Results concerning the domain size ($\langle D\rangle_s$ and $\langle D\rangle_v$) and the strain ($\langle\varepsilon_L^2\rangle^{1/2}L = 100$ Å and e) obtained from the multiple-line Voigt method are summarized in Table 3 and results concerning the column length distributions and strain ($\langle\varepsilon_L^2\rangle^{1/2}$) as a function of L are presented in Fig. 6. The high efficiency of the ball milling process on

Table 3
Results for the surface-weighted, volume-weighted domain sizes, RMSS and maximum strain from the "double Voigt" method

Disk speed (Ω) (rpm)	$\langle D\rangle_s$ (Å)	$\langle\varepsilon_L^2\rangle^{1/2}L =$ 100 Å (10^{-3})	$\langle D\rangle_v$ (Å)	e (10^{-3})
Starting powder	1013	1.1	1892	0.941
150	499	1.65	695	0.913
250	284	2.2	426	1.93
350	142	4	197	4.62

the domain size reduction has been noticed whatever the method employed (surface or volume-weighted). As it was expected the column length distribution becomes sharper when the disc speed increases. Furthermore the augmentation of the strain with the milling conditions has also been observed and it seems that a gap exists between the 250 and 350 rpm disk speed.

At this stage and using the properties of the Voigt functions, we are able to calculate the diffracting domain size and the lattice strain following five different methods:

(i) The simple Scherrer–Stoke relations using the integral breadth (Eqs. (1) and (2)) where the broadening of the peak is attributed to the sole size effect or to the sole strain effect. Assuming that the crystallites are quasi-isotropic an average of all the reflections can be made.
(ii) The Williamson–Hall plot using the integral breadth.
(iii) The Voigt method where the Cauchy component of the integral breadth is attributed the size effect and the Gauss component is attributed to the strain effect. Here again an average of all the reflections can be made.
(iv) The so-called "double Voigt" method that is used to determine the size and the strain Fourier coefficients (A_L^S, $\langle\varepsilon_L^2\rangle^{1/2}$) necessary to perform a Warren–Averbach line profile analysis. The results obtained by this method are then related to the direction normal to one family of plane, here the (1 1 0) one.
(v) The so-called "double Voigt method" which is used to determine the volume-weighted domain size $\langle D\rangle_v$, and the strain e consistent with the Scherrer–Stokes formalism but calculated using the β_{CS}, β_{CD}, β_{GS}, β_{GD} parameters. Here again the results are related to the direction normal to one family of plane.

According to the kinematic description of mechanical alloying [32,33] we have calculated the shock power, being the product of the frequency with the kinetic energy, generated in our system with our conditions. Indeed the shock power is a more meaningful physical parameter than the disk and the vial speeds. The values of the mechanical parameters for the different disk speeds are presented in Table 4.

We have then plotted in Figs. 7 and 8 the grain size and the strain as a function of the shock power for the single line methods (methods i, ii and iii) and for the multiple-line methods (methods iv and v). In Fig. 7, the methods are

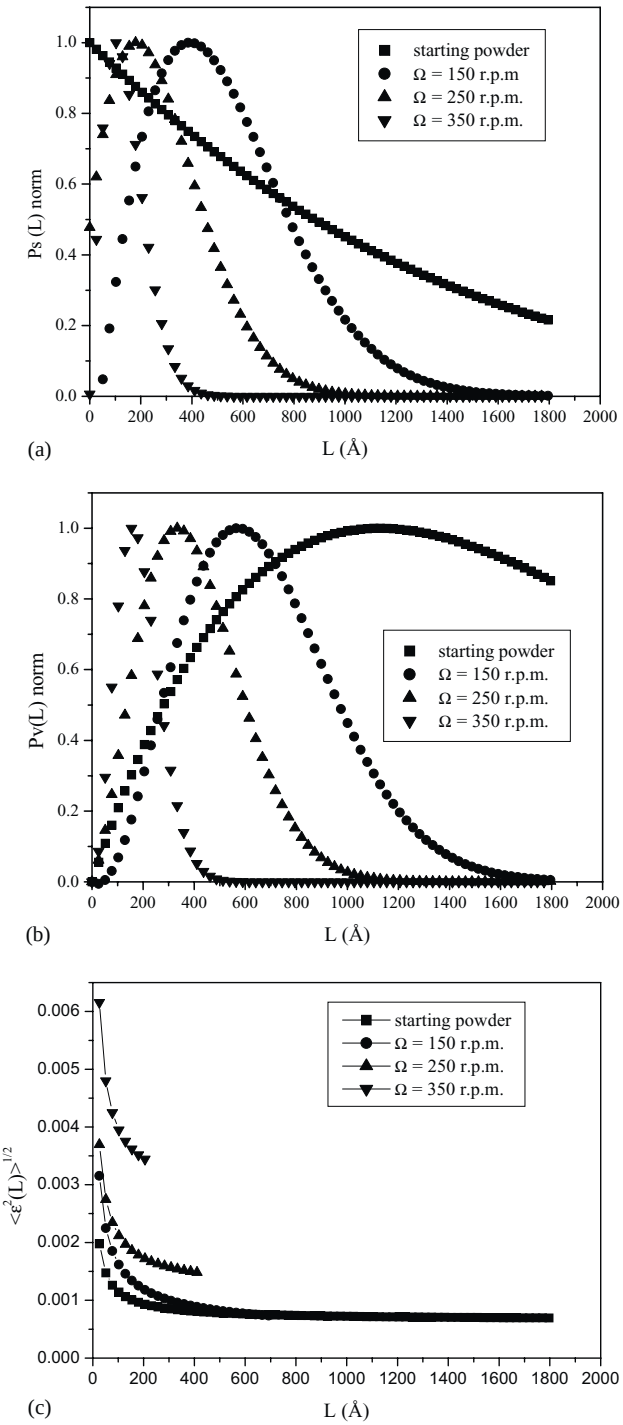

Fig. 6. Surface-weighted (a), volume-weighted (b), column length distribution functions and strain (c) as a function of L.

compared taking into account all the diffraction peaks and in Fig. 8 are presented the results concerning the plane (1 1 0).

Among all these methods the Williamson–Hall plot gives the highest values of the size and the lowest values of the strain of the crystallites. It has to be noted that in Fig. 7b the value of the maximum strain e is given thus the values of the strain η given in Table 2 concerning the Willamson–Hall

Table 4
Values of the shock power and the friction energy ratio for the various disk speed conditions

Disk speed (Ω) (rpm)	Shock power (W)	E_s/E_t
150	1.75	0.0917
250	3.63	0.7552
350	14.33	0.3935

plot have been divided according to the Eq. (4). Concerning the others averaged single line methods (Fig. 7) the Scherrer relations seems to under-estimate the size and over estimate the strain if it is compared to the Voigt method. This is due to the fact that in the Scherrer case all the peak broadening is attributed to the size or to the strain effect.

When we compare the results on the (1 1 0) plane (Fig. 8a), the $\langle D \rangle_v$ values and the Voigt (1 1 0) values are the largest. For these methods the calculation used the gauss component of Voigt functions coming from single (Voigt (1 1 0)) or

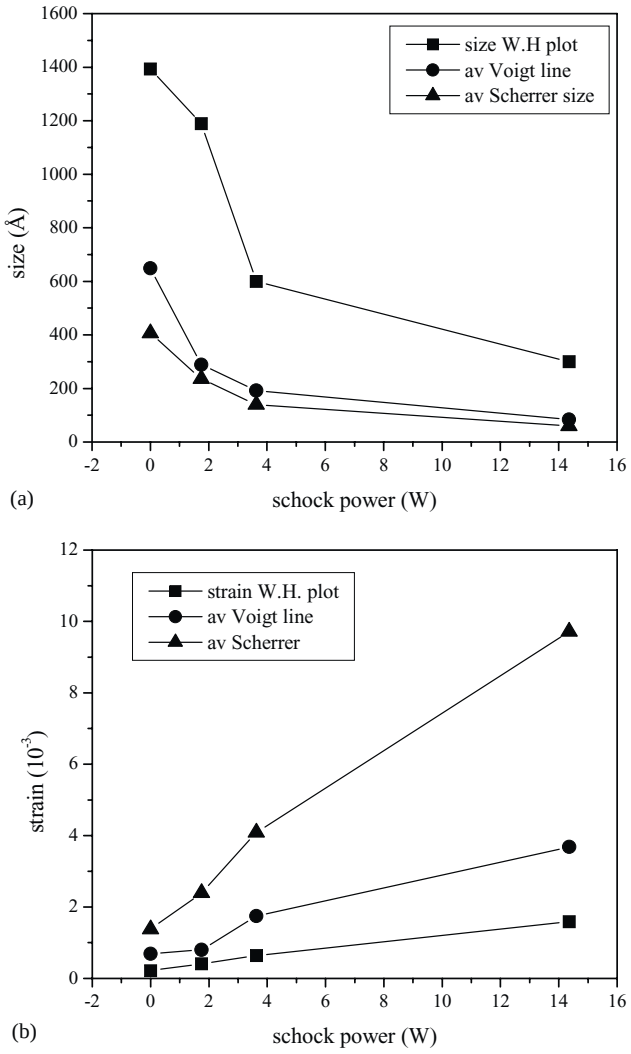

Fig. 7. Average values from all the diffraction peaks: (a) size and (b) strain.

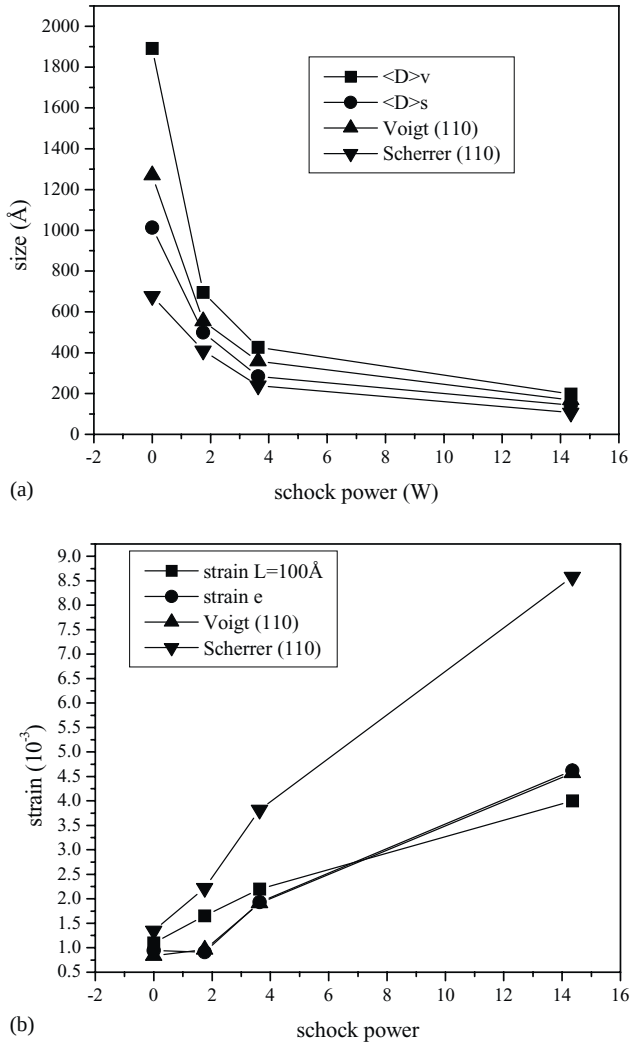

Fig. 8. Values for the (1 1 0) plane: (a) size and (b) strain.

multiple ($\langle D\rangle_v$) lines method. It has to be noticed (Fig. 8b) that the strains determined from these methods are very close. Here again the Scherrer relation and the maximum strain relation give the smallest size and the largest strain. These two figures illustrate the great discrepancy of the results obtained with different methods. Table 5 shows the comparison of the ratio between the highest and the lowest value of size and strain for all the methods and excluding the Williamson–Hall and the Scherrer–Stokes methods. As it can be seen more homogeneous results are obtained comparing Voigt and double Voigt methods than comparing all the methods.

Table 5
Ratio between the highest and the lowest value of the size and strain analysis for all the methods employed and excluding Williamson–Hall (WH) and Scherrer–Stokes (S) methods

Shock power (W)	Size	Size excluding WH and S	Strain	Strain excluding WH and S
0 (starting powder)	4.6	2.9	6.5	1.6
1.75	5	2.4	5.8	2.05
3.63	4.3	2.2	6.4	1.25
14.33	5	2.4	6.1	1.25

Assuming that strain broadening is due to the creation of dislocations we have analyzed X-rays diffraction results according to the model proposed by Ungar et al. [34]. This model is based on the modification of the Williamson–Hall plot.

$$\Delta K = \alpha + \beta K \bar{C}^{1/2} + O(K^2\bar{C}) \tag{16}$$

where $K = 2\sin(\theta)/\lambda$, ΔK is the FWHM, $\alpha = 0.9/D$ and β the constant depending on the effective outer cut-off radius of dislocations, on the Burgers vector and on the density of dislocations. $\bar{C}$ is the average contrast factor of dislocations and can be calculated following the relation:

$$\bar{C} = \bar{C}_{h00}(1 - qH^2) \tag{17}$$

with $H^2 = (h^2k^2 + h^2l^2 + k^2l^2/(h^2 + k^2 + l^2)^2)$.

$\bar{C}_{h00}$ values have been calculated in [34] for bcc systems as a function of elastic constant c_{11}, c_{22} and c_{44}. q is related to the nature of the dislocations (screw or edge) and values of q have been calculated for pure screw and pure edge dislocations as a function of the elastic constants in the bcc system. On the other hand, q can be deduced directly from the line profile analysis of the diffraction pattern. Indeed inserting (17) into the quadratic form of (16) yields

$$\frac{(\Delta K)^2 - \alpha}{K^2} = \beta\bar{C}_{h00}(1 - qH^2) \tag{18}$$

From the linear regression of the left-hand side of Eq. (18) versus H^2, the parameter q can be determined. We have thus determined the q parameter for each sample as it is illustrated in Fig. 9 and we have plotted the q values versus the shock power (Fig. 10). In Fig. 9, the values used for the calculation of the q parameter for pure edge and pure screw dislocations are $2c_{44}/(c_{11} - c_{12}) = 2.416$ and $c_{12}/c_{44} = 1.215$. We thus

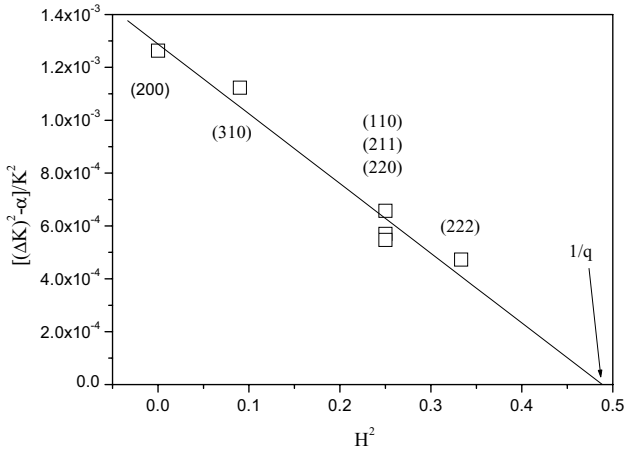

Fig. 9. Determination of the parameter q for the sample $\Omega = 350$ rpm.

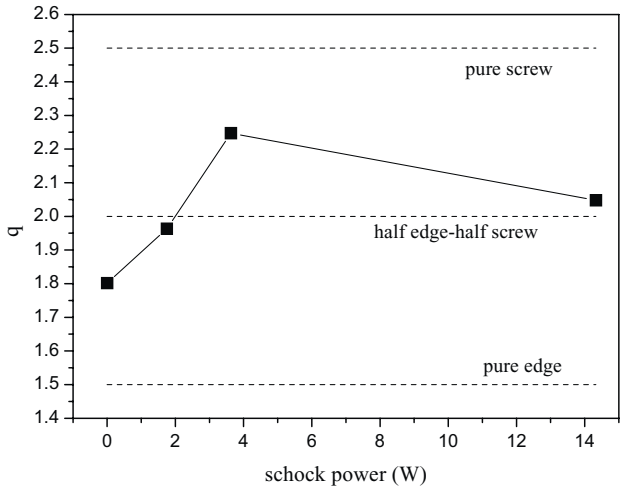

Fig. 10. Nature of the dislocations as a function of the shock power.

note that the screw nature of the dislocations increases until the 3.6 W condition and decreases for the 14.3 W condition.

In the ball milling process, the total kinetic energy E_t during the shock can be decomposed in two components [12]:

- The friction kinetic energy E_f proportional to the tangential velocity.
- The shock energy E_s proportional to the normal velocity.

As it can be seen in Table 4, the modification of the sole disk speed parameter greatly affects the shock power value and the ratio E_s/E_t. Furthermore these two parameters evolve in a different way as a function of the disk speed, the shock power increases with the disk speed while a maximum of the ratio E_s/E_t is reached for the 250 rpm condition.

We have plotted in Fig. 11 the q values as a function of the ratio E_s/E_t. It seems that the ratio of shock energy (or the ratio of friction energy which is the counterpart) governs the nature of the dislocations. Indeed when this ratio increases the nature of the dislocations goes from mainly edge to mainly screw. On the other hand, this ratio is not related to the number of dislocations meaning that even if the ratio E_s/E_t is larger for the $\Omega = 250$ rpm condition than for the $\Omega = 350$ rpm condition, we have no information, at this stage, about the density of dislocations for these conditions.

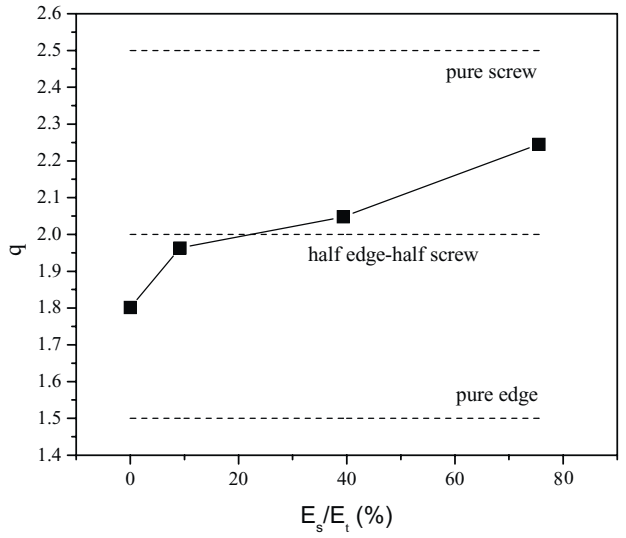

Fig. 11. Nature of the dislocations as a function of E_s/E_t.

In order to quantify the dislocations density we have employed the modified Warren–Averbach method [15]:

$$\ln A(L) \cong \ln A^{S}(L) - \rho B L^2 \ln\left(\frac{R_e}{L}\right)(K^2\bar{C}) + O(K^4\bar{C}^2) \quad (19)$$

ρ is the density of dislocations, $B = \pi b^2/2$ with b the Burgers vector of dislocations and O stands for higher order terms in $K^2\bar{C}$. Due to the equipment used in this study, the raw data are not of high quality to perform a correct Fourier analysis. Thus we have fitted the all the peaks by Voigt functions and used the properties of these functions to determine the Fourier coefficients. Indeed the Fourier transform of a Voigt function is expressed in (13) replacing A_S^L by $A(L)$ and β_{CS} and β_{GS} by β_C and β_G, respectively. Assuming an isotropic shape of the domains $\ln A(L)$ is then plotted for all the reflections and not only for two orders of one reflection. The term $X(L) = \rho B L^2 \ln(R_e/L)$ is determined from Eq. (19) for each L value. The values of ρ and R_e are obtained by plotting $X(L)/L^2$ versus $\ln(L)$ and by using a linear regression for the small values of L. Moreover following the modified Warren–Averbach method and using the plot $A_S(L)$ versus L we obtained a value of the domain size $\langle D\rangle_s$. The modified Warren–Averbach plot and the plot of $X(L)/L^2$ versus $\ln(L)$ for the 1.75 W condition are presented in Fig. 12. A summary of the density of dislocations and of the domain size (for the modified and classical Warren–Averbach and Williamson–Hall methods) is listed in Table 6. We note that the values of the domain size are close to those found using the classical Warren–Averbach method letting suppose a quasi-isotropic shape of the crystallites while the results are different for the classical and modified Williamson–Hall plots. The density of dislocations seems to reach a maximum for the 3.63 W condition and then decreases for the 14.33 W condition. On the other hand, we have seen that the strain still increases between those two conditions whatever is the method employed for it determination. It suggests that others sources of strain are present as stacking fault, twins or vacancies [16]. Considering the distance between dislocation $\delta = \rho^{-0.5}$ it comes that the average number of dislocation per crystallite is 22 for the starting powder and the 1.75 W condition, 18 for the 3.63 W condition and 7 for the 14.33 W condition.

As we have seen in this study, different approaches can be adopted to extract information about size and strain from diffraction patterns. Each method has advantages and

Table 6
Dislocations density and domain size following the modified and the classical Warren–Averbach and Williamson–Hall methods

Shock power (W)	ρ (10^{17} m^{-2})	$\langle D\rangle_s$ (Å) modified WA	$\langle D\rangle_s$ (Å) classical WA	$\langle D\rangle_v$ (Å) modified WH	$\langle D\rangle_v$ (Å) classical WH
0 (starting powder)	0.46	1046	1013	960	1393
1.75	1.53	567	499	796	1189
3.63	2.98	335	284	380	600
14.33	2.6	145	142	292	300

disadvantages. For a rapid comparison, the Scherrer–Stokes formalism is still very useful even if this method leads to erroneous results. The Williamson–Hall plot allows the effects of size and strain to be separated, but is valid only if the data follow a straight line. If this is not the case, some data have to be excluded or linear fits have to be performed for different families of planes [21]. As we have shown, Voigt methods and Warren–Averbach formalism lead to homogeneous results and have to be employed to extract accurate information about size and strain of diffracting domains. The main differences between these methods are as follows:

- One of these methods take into account all the diffraction peaks (Voigt method) and implies averaged values assuming an isotropic shape of the diffracting domains, while the other is related to one family of planes (Warren–Averbach).
- These methods are based on different definition of the size and the strain (volume-weighted or surface-weighted size and apparent or RMS strain). $\langle D\rangle_v$ is always greater than $\langle D\rangle_s$ with $1.31 \leq (\langle D\rangle_v/\langle D\rangle_s) \leq 2$ [29,35] and in the case of pure Gauss strain broadening $\langle \varepsilon_L^2\rangle^{1/2} = (2/\pi)^{1/2} e$ [29,35].

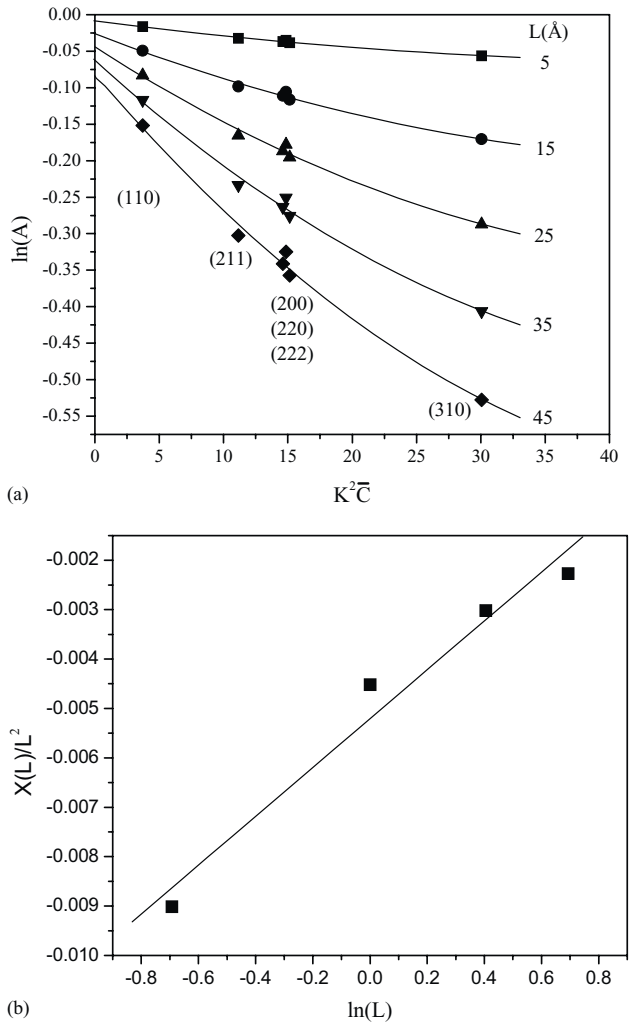

Fig. 12. Modified Warren–Averbach plot (a) and plot of $X(L)/L^2$ vs. ln(L) (b) for the 1.75 W condition.

4. Conclusion

We have described and employed different line profile analysis methods to determine the size of coherently diffracting domains and the lattice strain of ball milled powders. Voigt functions have been used to fit all the diffraction peaks. Whatever the method employed the efficiency of ball milling has been evidenced. Among these methods the so-called "double Voigt" one allows to have analytical expression of the Fourier coefficients used in the Warren–Averbach. All the methods display the same trend:

- Rapid decrease of the coherently diffracting domain size.
- Increase of the strain state.

Willamson–Hall, Scherrer and apparent strain relations have to be employed only in a first qualitative approximation, more accurate results are obtained using the single line Voigt or the so-called "double Voigt" methods.

We have used the shock power and the ratio E_s/E_t, which are meaningful physical parameters, instead of the classical disk speed to compare ours results.

Assuming that the strain is only due to dislocations we have used the average contrast factor of dislocations and the modified Williamson–Hall plot to evaluate the screw or the edge nature of these dislocations as a function of the shock power. We have noted the increase of the screw nature up to a maximum (3.6 W) and a decrease for the highest shock power condition (14.3 W). We have also observed that the ratio of the shock energy E_s/E_t seems to govern the nature of the dislocations (edge or screw).

Finally the density of dislocations have been determined according to the modified Warren–Averbach method, we have then noted a maximum value ($2.98 \times 10^{17}\ m^{-2}$) for the 3.6 W condition.

References

[1] P. Scherrer, Nachr. Ges. Wiss. Göttingen. 26 (1918) 98.
[2] E.M. Gonzales, M.I. Montero, F. Cebollada, C. DE Julian, J.L. Vincent, J. M Gonzalez, Europhys. Lett. 42 (1) (1998) 91.
[3] F. Zhou, H.W. Sheng, K. Lu, J. Mater. Res. 13 (2) (1998) 249.
[4] M. Zdujic, C. Jovalekic, Lj. Karanovic, M. Mitric, Mater. Sci. Eng. A262 (1999) 204.
[5] H.J. Ryu, S.H. Hong, W.H. Baek, Mater. Sci. Eng. A291 (2000) 91.
[6] J.S.C. Jang, H.P. Shih, Mater. Chem. Phys. 70 (2001) 217.
[7] C.N. Chinnasamy, A. Narayanasamy, N. Ponpandian, K. Chattopadhyay, M. Saravanakumar, Mater. Sci. Eng. A304–A306 (2001) 408.
[8] A.C.J. Wilson, Mathematical Theory of X-ray Powder Diffractometry, Philips, Eindhoven, 1963.
[9] A.R. Stokes, A.C.J. Wilson, Proc. Phys. Soc. London 56 (1944) 174.
[10] G.K. Williamson, W.H. Hall, Acta. Metall. 1 (1953) 22.
[11] A. Munitz, G. Kimmel, J.C. Rawers, R.J. Fields, Nanostruct. Mat. 8 (7) (1997) 867.
[12] I. Borner, J. Eckert, Mater. Sci. Eng. A226–A228 (1997) 541.
[13] N.R. Rochma, K. Kawamoto, H. Sueyoshi, Y. Nakamura, T. Nishida, J. Alloys Comp. 89–90 (1999) 367.
[14] J. Li, F. Li, K. Hu, Y. Zhou, J. Alloys Comp. 3334 (2002) 253.
[15] H.J. Niu, D.P. Hampshire, Phys. C 372–376 (2002) 1145.
[16] M. Krasnowski, A. Witek, T. Kulik, Intermetallics 10 (2002) 371.
[17] H. Mandar, J. Felsche, V. Milki, T. Vajakas, J. Appl. Cryst. 32 (1999) 345.
[18] Y.H. Dong, P. Scardi, J. Appl. Cryst. 33 (2000) 184.
[19] J.I. Langford, J. Appl. Cryst. 11 (1978) 10.
[20] T.H. De Keijser, J.I. Langford, E.J. Mittemeijer, B.P. Vogels, J. Appl. Cryst. 15 (1982) 308.
[21] J.I. Langford, in: E. Prince, J.K. Stalick (Eds.), Accuracy in Powder Diffraction II, NIST Special Publication 846, USG Printing Office p110, Washington, 1992.
[22] B.E. Warren, X-ray Diffraction, Addison-Wesley, New York, 1970.
[23] E. Bonetti, L. Del Bianco, L. Pasquani, E. Sampaolesi, Nanostruct. Mat. 10 (5) (1998) 741.
[24] H.H. Tian, M. Atzmon, Acta. Mat. 47 (4) (1999) 1255.
[25] E. Bonetti, L. Del Bianco, L. Pasquani, E. Sampaolesi, Nanostruct. Mat. 12 (1999) 685.
[26] P. Baviera, S. Harel, H. Garem, M. Grosbras, Scripta Mater. 44 (2001) 2721.
[27] S. Bid, A. Banerjee, S. Kumar, S.K. Pradhan, U. De, D. Banerjee, J. Alloys Comp. 326 (2001) 292.
[28] A.R. Stokes, Proc. Phys. Soc. London 61 (1948) 382.
[29] D. Balzar, in: R.-L. Snyder, H.J. Bunge, J. Fiala (Eds.), Defect and Microstructure Analysis from Diffraction, International Union of Crystallography Monographs on Crystallography, vol. 10, Oxford University Press, New York, 1999, p. 94.
[30] A. Revesz, T. Ungar, A. Borbely, J. Lendvai, Nanostruct. Mat. 7 (1996) 779.
[31] T.R. Mallow, C.C. Koch, Acta Mater. 45 (5) (1997) 2177.
[32] M. Abdellaoui, E. Gaffet, Acta Mater. 44 (2) (1996) 725.
[33] M. Abdellaoui, E. Gaffet, J. Alloys Comp. 209 (1994) 351.
[34] T. Ungar, I. Dragomir, A. Revesz, A. Boberly, J. Appl. Cryst. 32 (1999) 992.
[35] T.H. De Keijser, E.J. Mittemeijer, H.C.F. Rozendaal, J. Appl. Cryst. 16 (1983) 309.